Segregation and periodic mixing in a fluidized bidisperse suspension

2011 New J. Phys. 13 075005

(http://iopscience.iop.org/1367-2630/13/7/075005)

New Journal of Physics
The open-access journal for physics

Segregation and periodic mixing in a fluidized bidisperse suspension

A Deboeuf, G Gauthier, J Martin[1] and D Salin

Univ. Pierre et Marie Curie, Univ. Paris-Sud, CNRS, UMR 7608, Lab. FAST, Bat. 502, Campus Univ., Orsay F-91405, France
E-mail: martin@fast.u-psud.fr

New Journal of Physics **13** (2011) 075005 (19pp)
Received 12 January 2011
Published 15 July 2011
Online at http://www.njp.org/
doi:10.1088/1367-2630/13/7/075005

Abstract. We address the issue of segregation in bidisperse suspensions of glass beads, by using a liquid fluidized bed in the inertialess regime and an acoustic technique for acquiring the axial composition along the column. Fluidization balances the buoyancy of the particles by a constant uniform upward flow, and therefore enables long-time experiments. From the analysis of the transient segregation fronts, we have collected precise measurements on the sedimentation velocities of small and large beads, U_s and U_l, in homogeneous suspensions at the same volume fraction, $\bar{\Phi}/2$, for both the bead species, and for different size ratios, $1.13 \leqslant \lambda \leqslant 1.64$, and solid concentrations, $25\% \leqslant \bar{\Phi} \leqslant 50\%$. Our measurements provide evidence for a difference in the sedimentation velocities, U_s and U_l, over all the ranges of λ and $\bar{\Phi}$ covered. These results make one expect that a long-term fluidization should then result in a stationary segregated state, which was indeed always obtained for large enough particle size ratios, $\lambda \geqslant 1.43$. However, at high concentration and for particles of close sizes, $\lambda \leqslant 1.41$, we observed a surprising pseudo-periodic intermittency of slow segregation and quick mixing phases. The intermittency time is much longer than the batch sedimentation time and becomes noisy at very high concentration, for which metastable states have been observed. The origin of the mixing destabilization remains an open issue, but we note however that the domain of occurrence, $\lambda \leqslant 1.41$, also corresponds, in our experiments, to a continuous size distribution of the particles.

[1] Author to whom any correspondence should be addressed.

Contents

1. Introduction

Sedimentation and fluidization are used in many fluid processes (water purification, smoke purification, reprocessing of nuclear waste, chemical reaction, particle sizing, etc), and although they have been studied for a long time, their behavior in the presence of polydispersity are still intriguing. However, it is known that at low Reynolds number batch sedimentation of monodisperse particles in a Newtonian fluid, the settling velocity is the result of a balance between buoyancy and viscous forces; the larger the particles, the faster their settling velocity; the larger the concentration, the larger the hindrance due to back-flow and therefore the slower the settling velocity. Moreover, this batch sedimentation of identical spherical non-colloidal particles is stable in the absence of inertia [1]. Indeed, in a sedimentation process, any concentration (i.e. density) inhomogeneity in a horizontal plane will induce velocity fluctuations (hydrodynamic dispersion) [2, 3] which will tend to damp the inhomogeneities. As a result, monodisperse suspensions become quickly uniformly distributed in any horizontal plane, and their evolution can be accounted for by an axial description [4]. Such a description has been applied extensively to either batch sedimentation [5, 6] or fluidization [7] of monodisperse suspensions. It has also been extended to the case of polydisperse suspensions to address the issue of axial segregation, in particular for the case of bidisperse suspensions [8]. However, the axial description requires the flux functions for the different species, and even for the simple case of bidisperse suspensions, their expressions are still an open issue. Numerous models and expressions have been proposed for these functions of the concentrations of the two particulate species, their Stokes velocity, their density contrast and their size ratio [9–20]. Most of these models predict an axial segregation in accordance with the hierarchy of the Stokes velocities: during batch sedimentation, the slowest particles (i.e. the smallest or lightest ones) should be driven across the top front of a bidisperse sedimenting suspension. At the same time, measurements lead to various results [13, 18], [20–26], which makes it difficult to discriminate between the different models. Moreover, some experimental [27–29] and numerical [30] works

on bidisperse sedimentation have reported on the presence of a streaming instability. Although the onset of such an instability may be explained in the framework of the axial model [29, 31], as the hyperbolic–elliptic transition of the set of equations describing the evolution of the system [32], it is clear that the development of a streaming pattern should invalidate the axial description and require a more sophisticated model. This should be the case for suspensions presenting a density contrast between particles, for which either streaming in sedimentation [27–29] or layer inversion in fluidization [33, 34] has been reported. In the absence of density contrast between particles, however, such phenomena should not appear [29, 34], and the axial description should apply. The size difference between the particles should then induce segregation, at least for a small enough volume fraction of the particles [9, 10]. In the concentrated regime, we note that an inhibition of the segregation process was reported for a size ratio $\lambda = 1.68$ and for an overall volume fraction $\Phi > 0.45$ [26], whereas recent experiments [35] have evidenced some segregation for a size ratio, λ, as small as 1.05, and volume fractions, Φ, as large as 50%. We note that this segregation inhibition issue is, however, difficult to address through batch sedimentation experiments, as the segregation velocity at high concentration becomes so small that a segregated layer is usually hardly formed within the experimentation time. We re-examine the segregation issue at large volume fractions in a liquid fluidized bed. Such a device enables long-time experiments, and is known to provide, at low Reynolds number, a stable stationary sedimenting suspension [36, 37]. For a bidisperse suspension, an achieved segregated state is then expected. We note that at small volume fraction ($\Phi < 15\%$), a stationary partially segregated state has been observed, associated with a concentration gradient all along the column of fluidization [38, 39]. In the present study, we address the issue of segregation inhibition and focus on larger volume fractions in the range $25\% < \Phi < 50\%$. The concentration of both species is determined thanks to an acoustic technique [26, 36, 40]. In agreement with previous batch sedimentation experiments, we observe segregation for large enough particle size ratios. However, for particles of close sizes and at high concentration, where the issue of segregation inhibition arises, the fluidization of the bidisperse suspension results in totally unexpected behavior, namely a quasi-periodic intermittency of segregation and mixing phases.

2. Experimental setup

2.1. The fluidized bed and the acoustic technique

A sketch of the experimental setup is displayed in figure 1. The fluidization column is 50 cm high and has a uniform internal section, S, of 4 cm width and 1 cm thickness. The walls are made of 8 mm-thick polycarbonate plates. A polypropylene porous filter ensures a uniform fluid injection at the bottom of the cell. The top of the column is open to enable us to add, remove or stir up the suspensions. A pair of moving acoustic transducers enables exploration of the vertical composition of the bed along the center of the cell. The system measures the delay and amplitude of a 3 MHz sine pulse transmitted across the cell. The 3 MHz frequency was selected in order to optimize the sensitivity of the attenuation to the particle size, while keeping a measurable signal. The latter constraint requires an acoustic impedance matching, which also avoids signal interferences. This matching is obtained by immersing the transducers and polycarbonate cell in a thermostatic water bath, at $T = 20\,^{\circ}\mathrm{C}$. Note that the temperature control also fixes the sound velocity and viscosity of the suspending fluid. The spatial resolution

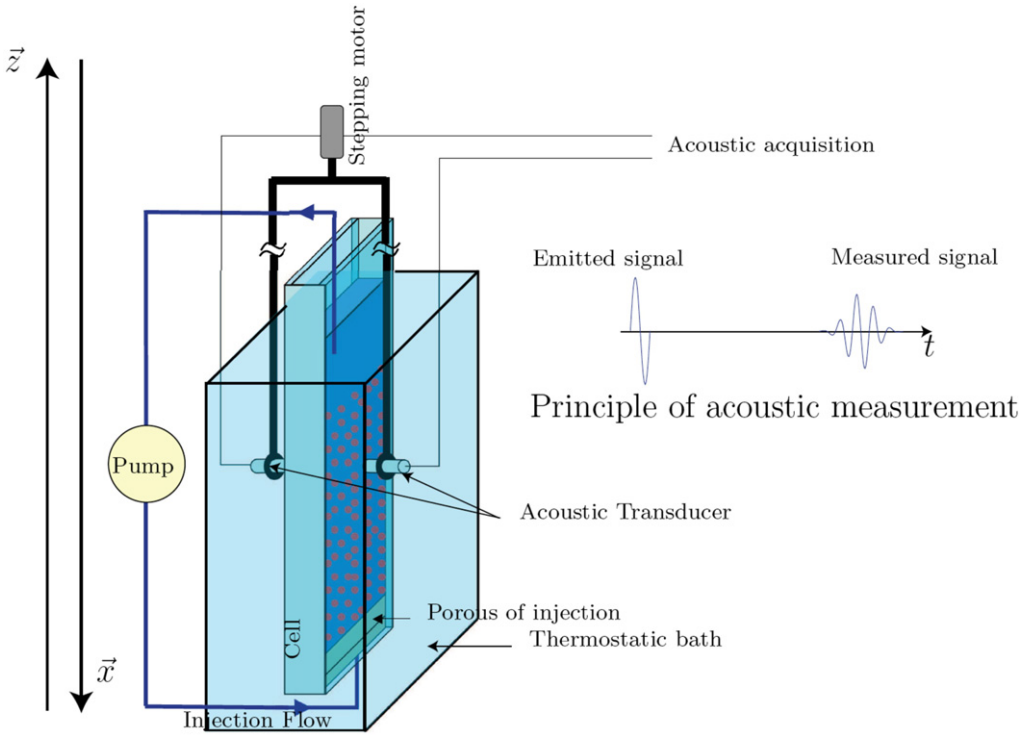

Figure 1. Experimental setup of the fluidization column.

lies between the scan step, 2 mm, and the transducers diameter, 12 mm. For the sake of accuracy, the acoustic measurements are averaged over 500 signals, which requires 9 s for each scan step and results in a typical scan duration of around 10 min (≈60 measurement locations). Such a procedure enables us to get rid of any radiative noise emitted by the brushless motor of the scanner and does not wipe out any accessible physical phenomenon, as the maximum displacement of any bead during the averaging procedure (evaluated with the largest Stokes velocity, u_1, reported in table 1) remains smaller than the transducer diameter.

The suspending fluid is a water–glycerol mixture of density $\rho = 1.19\,\mathrm{g\,cm^{-3}}$ and viscosity $\eta = 30 \pm 1\,\mathrm{mPa\,s}$. It is newtonian and thick enough to provide stable inertialess fluidization [7, 36, 37].

2.2. *Monodisperse calibration*

Monodisperse suspensions were prepared by mixing 30 g of sieved spherical glass beads, of density $\rho = 2.5\,\mathrm{g\,cm^{-3}}$, with the suspending fluid. The so-obtained monodisperse suspensions were first degassed and calibrated in the fluidized bed. The bidisperse suspensions were then obtained by mixing one monodisperse suspension of small beads, with one suspension of large beads. Five different sets of small beads were used, the sizes of which are reported in table 1, with the same set of large ones, in suspensions 1–5. The resulting size distributions, measured with a Malvern Morpho G3 and displayed in figure 2, are indicated in the second column of table 1. Note that the earliest studies were carried out with another bidisperse suspension (6, last row), with slightly smaller large beads, and for which the size distribution analysis is unfortunately unavailable.

Table 1. Characteristics of the bidisperse suspensions: the mean diameters a_s, a_l, with their standard deviations, obtained from a size analysis of the bidisperse suspensions, the Stokes velocities, u_s and u_l, and the exponents n_s and n_l, obtained from Richardson–Zaki fits of the monodisperse suspensions, and the size ratio λ, estimated with the Stokes velocities.

Suspension	a_s (μm)	a_l (μm)	u_s (mm s^{-1})	u_l (mm s^{-1})	n_s	n_l	Size ratio $\lambda = \sqrt{u_l/u_s}$
1	120 ± 6.5	197 ± 3.6	0.42	1.12	5.15	5.15	1.64
2	144 ± 4.1	197 ± 4.3	0.50	1.12	4.93	4.95	1.50
3	155 ± 3.9	197 ± 5.0	0.55	1.12	5.02	4.95	1.43
4	170 ± 6.6	196.5 ± 6.0	0.56	1.12	4.93	4.95	1.41
5	173 ± 6.0	196 ± 5.2	0.61	1.12	4.89	4.95	1.36
6			0.635	0.817	4.90	5.10	1.13

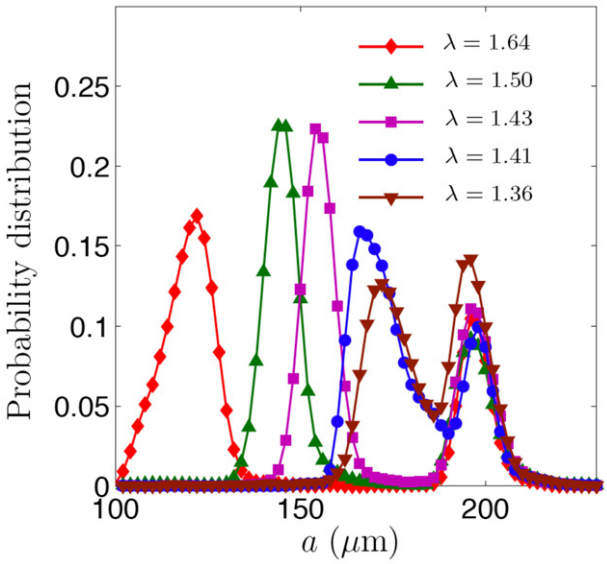

Figure 2. Size distributions of the bidisperse suspensions.

Prior to the bidisperse studies, the monodisperse suspensions were systematically calibrated. Different constant volumetric flow rates Q were applied, to get stationary homogeneous fluidized suspensions of different volume fractions Φ (measured from the height of the bed), in the range $0.25 < \Phi < 0.55$. Note that each upward surface flow rate, $q = Q/S$, was characterized with the following procedure. The inlet of the pump was abruptly connected to an external fluid vessel (thanks to a bypass, not displayed on the diagrammatic sketch of figure 1), and the fluid on top of the fluidized suspension was mostly removed. Then the fluid level in the cell was recorded. Its upward velocity, $q = Q/S$, was measured and found to be constant, i.e. independent of pressure head variations of typically 100 Pa (corresponding to fluid level variations of 10 cm in the cell). After such a q calibration procedure, the inlet of the pump was reconnected to the top of the cell, to close the hydraulic circuit. For each stationary state, an acoustic scan was realized. Figure 3 displays the resulting calibration curves of the

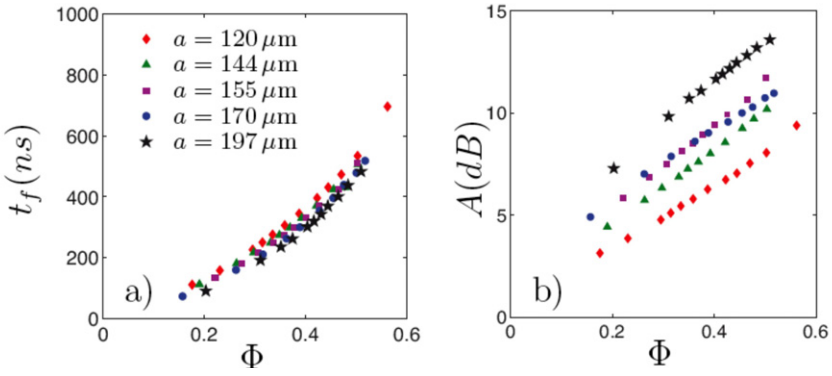

Figure 3. Variations, with the average volume fraction Φ, of the time-of-flight t_f and of the attenuation A of a 3 MHz acoustic wave through a suspension of monodisperse glass beads, of diameters 120, 145, 155, 170 and 197 μm.

time-of-flight, t_f, and of the attenuation A. t_f denotes the difference between the flight duration measured in the pure fluid and that measured across the suspension, whereas, in a similar way, A denotes the excess of attenuation, measured in the presence of beads. We note that the different sets of t_f data differ only slightly: they collapse onto a main calibration curve $t_f(\Phi)$, which thus enables us to extract Φ values from t_f measurements [5]. Conversely, at the selected frequency, 3 MHz, A strongly depends on the particle size and thus provides the local relative composition once the volume fraction is known. As we will be mostly interested in the evolution of the axial composition of fluidized bidisperse suspensions, we will preferentially make use of the attenuation scans in the following.

Once the acoustic scans were realized on the stationary fluidized monodisperse suspensions, the flow rate was cut in order to measure the batch sedimentation velocity $U(\Phi)$, from the resulting top front displacement. As expected [36], the downward sedimentation velocity $U(\Phi)$ was found to equal the upward surface flow rate $q = Q/S$, and to obey a Richardson–Zaki law [41]:

$$q = U(\Phi) = u\,(1-\Phi)^n. \tag{1}$$

The fitting parameters, u and n, represent a Stokes velocity and the hindering function exponent, respectively, and are listed in table 1. Moreover, the square dependence of the Stokes velocity on the size of the particle enables us to define a 'hydrodynamic size ratio', $\lambda = \sqrt{u_l/u_s}$, reported in table 1, which we will use as a parameter in the following studies of bidisperse sedimentation. We note that in all our experiments, the particle Reynolds number $Re_p = \rho u_l a_l/\eta$ and the flow Reynolds number $Re = \rho q W/\eta$ (with W being the width of the cell) were lower than 10^{-3} and 0.6, respectively, so that inertia is expected to be negligible.

3. Segregation in bidisperse suspensions

3.1. Experiments

The bidisperse suspensions are prepared by mixing inside the fluidization cell two monodisperse suspensions containing 30 g of beads each. Then, at a given constant fluidizing flow, the bidisperse suspension is first manually stirred up. This results in a well-mixed suspension,

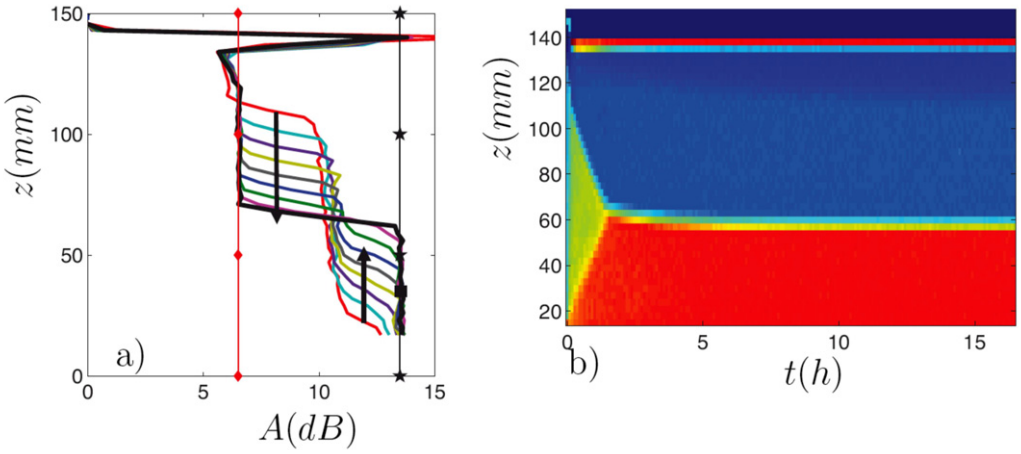

Figure 4. Attenuation profiles (left) and the corresponding spatiotemporal attenuation diagram (right) obtained with the bidisperse suspension 1, of diameters 120 and 197 μm ($\lambda = 1.64$, $q = 0.034\,\mathrm{mm\,s^{-1}}$ and $\bar{\Phi} = 0.43$). The profiles were measured every 330 s: the red curve is the first scan, the bold black one was obtained in the final stationary state and the vertical lines with symbols correspond to the attenuation values $A = 6.5$ and 13.5 dB, measured in the monodisperse suspensions of small and large beads, respectively, at the same flow rate.

at a volume fraction slightly lower than that expected from the upward flow. However, the stirring process is followed immediately by a fast settling of the suspension: the top front of the fluidized suspension moves down and then reaches a location fixed by the imposed flow rate, which remains nearly constant during the segregation phase. We note that the time resolution of our acoustic scanner does not enable us to catch the fast initial reconcentration, but is perfectly suitable to follow the dynamics of the subsequent segregation process. Figure 4 displays the successive attenuation scans obtained after the initial mixing, in the bidisperse suspension 1, at the fluidizing velocity $q = 0.034\,\mathrm{mm\,s^{-1}}$. Note first that the peaks measured in each scan at $z \simeq 140$ mm of the injection point are due to the interferences occurring when the transducers face the steep top front of the suspension. The constant location of the peaks corroborates our observation that the top front hardly moves during the segregation process. This means that the average volume fraction $\bar{\Phi}$, estimated from the height of the suspension, remains unchanged during the segregation, and can be used as a parameter to characterize the decompaction of the bidisperse bed. During the experiment of figure 4, although the average concentration remains constant at $\bar{\Phi} \simeq 0.43$, the attenuation profiles measured inside the fluidized suspension evidence the occurrence of a segregation process. The intermediate scans exhibit three successive plateaux of the attenuation value, at $A \simeq 6.5$, 10.5 and 13.5 dB, from the top to the bottom of the suspension. They correspond, respectively, to the attenuations of a monodisperse suspension of the small particles, of a well-mixed bidisperse suspension (the initial one), and to an attenuation very close to that of the monodisperse suspension of the large particles. These plateaux are separated by two rather steep internal fronts: one between the top suspension of small beads and the initial bidisperse suspension, which travels downwards (at a velocity denoted by v_d) as the top monodisperse suspension develops, and the other

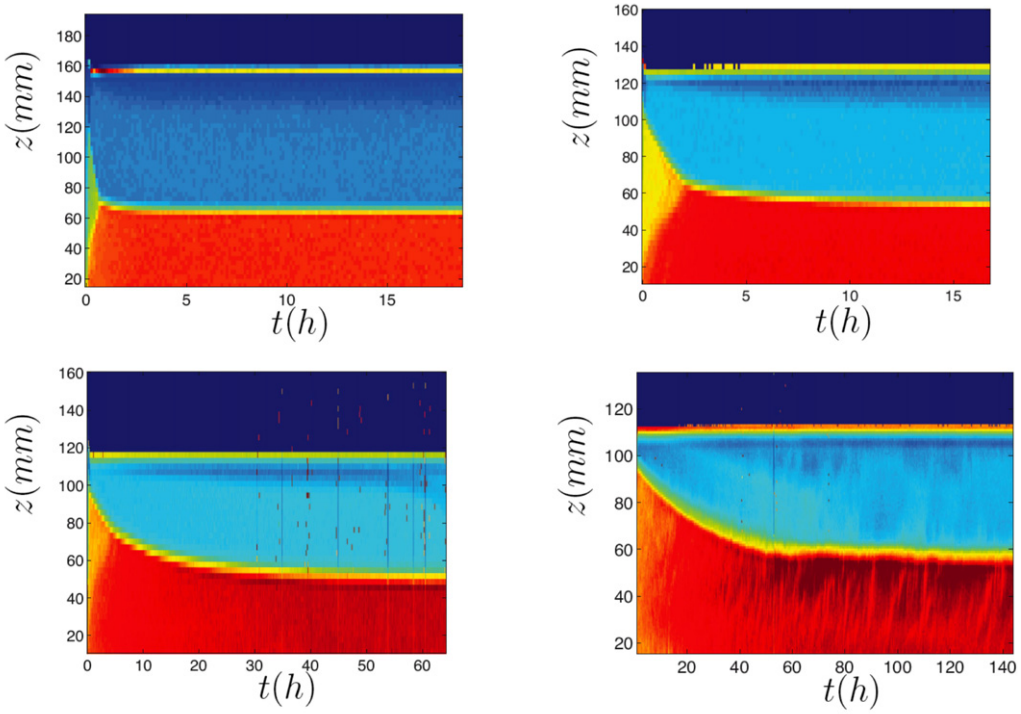

Figure 5. Spatiotemporal attenuation diagrams obtained with the bidisperse suspension 1, of diameters 120 and 197 μm ($\lambda = 1.64$), for $q = 0.052\,\mathrm{mm\,s^{-1}}$ ($\bar{\Phi} \simeq 0.38$), $q = 0.025\,\mathrm{mm\,s^{-1}}$ ($\bar{\Phi} \simeq 0.46$), $q = 0.016\,\mathrm{mm\,s^{-1}}$ ($\bar{\Phi} \simeq 0.51$) and $q = 0.011\,\mathrm{mm\,s^{-1}}$ ($\bar{\Phi} \simeq 0.54$), from left to right and top to bottom.

between the bidisperse suspension and the suspension enriched in large particles, which travels upwards (at a velocity denoted by v_u) as the bottom suspension region develops. A stationary segregated state is reached when the two fronts meet. This segregation process is even clearer on the spatiotemporal attenuation diagram, displayed on the right of figure 4, where the attenuation is coded in color. On the left side of the diagram, one can note, from bottom to top, the large beads suspension, the bidisperse one, the small beads suspension and the clear suspending fluid, in red, green, light blue and dark blue, respectively. The diagram clearly shows that the segregation process, achieved in about 2 h, results in a stationary fully segregated state. Note that this last point was confirmed by the measurement of the heights of suspensions, which were found to exactly fit the ones obtained in the monodisperse calibration, at the same flow rate q. The spatiotemporal attenuation diagram also enables us to conveniently measure the segregation velocities, v_d and v_u, from the slopes of the frontiers.

3.2. Segregation measurements

The evolution of the spatiotemporal attenuation diagrams measured in the suspension 1, for average volume fractions increasing from $\bar{\Phi} \simeq 0.38$ to $\bar{\Phi} \simeq 0.54$, is displayed in figure 5. A segregation phase is observed in the four diagrams, and its duration increases with $\bar{\Phi}$, as could be expected from hindrance considerations. Once again, the location of the top of the fluidized suspension (frontier between light and dark blue) hardly changes during the

segregation. However, a slight increase in the front location, i.e. a $\bar{\Phi}$ decrease, may be noted: the segregation results in an overall decompaction of the bidisperse suspension. The diagram sequence also displays an evolution of the segregation process as $\bar{\Phi}$ is increased. In the aforementioned process, observed at $\bar{\Phi} \simeq 0.43$ (figure 4) and $\bar{\Phi} \simeq 0.38$ (figure 5, top left), two frontiers are observed, between the initial bidisperse suspension and the suspensions of large beads (bottom) and small beads (top). These two frontiers are contrasted straight lines (constant slopes) between monochrome regions. This supports the contention that the bidisperse composition does not evolve as the segregation takes place and that the two front velocities, v_d and v_u, which remain constant, correspond to two shocks [4, 8]. However, these features do not hold true as the average concentration is increased. First, the upward front becomes less and less contrasted as $\bar{\Phi}$ increases above 0.46, and does not exist anymore at $\bar{\Phi} \simeq 0.54$. We note that a monodisperse suspension of small particles (homogeneous light blue) still develops in all cases. But for $\bar{\Phi} \simeq 0.54$, the bottom suspension (i.e. under the light blue region on the diagram) is almost homogeneous at each time step, but evolves continuously from the bidisperse initial composition toward a suspension of large beads. Hence, the downward front separates the small beads suspension forming at the top, from a bidisperse suspension of varying composition. Therefore, it does not represent the same shock as time elapses, and the corresponding shock velocity u_d does not remain constant; the frontier slope decreases during the segregation process. To complete the description of the experiment at $\bar{\Phi} \simeq 0.54$, we can also note the presence of nearly vertical stripes in the bottom suspension. This indicates that some small beads may remain in the bottom region of the column and generate small variations in the composition in the center plane of the cell.

The segregation processes were systematically studied for the six bidisperse suspensions listed in table 1. In suspensions 2–6, of lower size ratio λ, no upward front was observed in the explored concentration range. Moreover, in all cases, the downward front displayed some variations in its velocity, indicated by the bending of the frontier on the spatiotemporal attenuation diagrams. In order to get reliable data, we measured the velocity of the downward front, v_d, at the early stage of the segregation, just after the stirring and the initial suspension reconcentration. At this time, one can assume that the bidisperse suspension is homogeneous, at the initial composition:

$$\Phi_l = \Phi_s = \bar{\Phi}/2, \tag{2}$$

where Φ_l and Φ_s are the volume fractions of the large and small beads. Accordingly v_d represents the mean velocity of the large beads in the bulk of the initial fluidized bidisperse suspension. The values of v_d, measured along the downward vertical axis Ox, are displayed in figure 6(a). Whereas suspensions 1–3 and 3–5 contain the same large particles, their series differ significantly. For small values of $\bar{\Phi}$, v_d increases strongly with λ, for $\lambda \geqslant 1.43$. On the other hand, the values obtained for $\lambda = 1.41$ and $\lambda = 1.36$ compare very well, and are also close to the series $\lambda = 1.13$.

The velocities v_d for all the series tend to zero at high concentration, with a vanishing delayed from $\bar{\Phi} \simeq 45\%$ to $\bar{\Phi} \simeq 55\%$, as the size ratio is increased from $\lambda = 1.13$ to $\lambda = 1.64$. However, this apparent cancellation of the segregation velocity does not hold in figure 6(b), in which the data are normalized by q. Moreover, such a representation enables the differentiation of all the series, and shows that v_d does actually increase with λ, even for λ close to 1. We note that the surface flow rate q represents the mean sedimentation velocity of the bidisperse suspension (see the following equation (5)): it accounts for the typical Stokes velocities involved

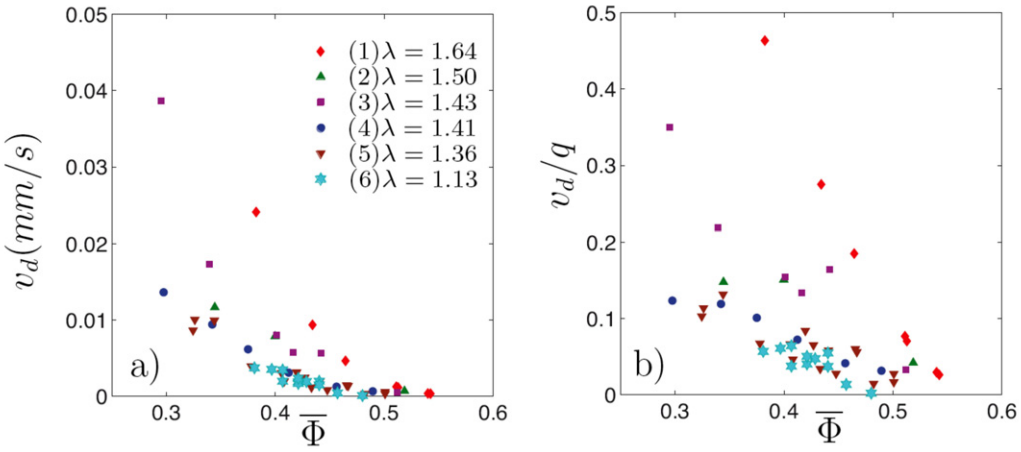

Figure 6. Segregation front velocities v_d, in mm s^{-1} (a) and normalized by q (b), measured at an early stage of the segregation process in bidisperse fluidized suspensions, of size ratio λ, initially uniform at volume fraction $\bar{\Phi}/2$ for each particle size.

in the suspensions (which differ for suspension 6) and for the 'effective hindering function' of the bidisperse suspension, which strongly increases at high concentration. Accordingly, the decrease of v_d with $\bar{\Phi}$ is diminished by the normalization by q, but we note that it remains significant in figure 6(b) and is therefore stronger than what one could have expected from simple hindrance considerations. However, figure 6(b) also shows that the normalized data do not cancel, whatever the value of λ is and even for $\bar{\Phi} > 50\%$. Moreover, the different series all separate, revealing an increase of v_d with λ, even for the smallest size ratios.

3.3. Segregation analysis

Whereas the quantitative measurements of v_d displayed in figure 6 can allow comparison with various models of segregation in fluidized beds, we note that sedimentation models usually predict the batch sedimentation velocities of the different particles. The latter, denoted by U_l and U_s in our bidisperse suspensions, represent the average velocities of the large and small beads, respectively, in a suspension of volume-averaged velocity equal to zero (batch sedimentation condition). For the sake of comparison, one must account for the volume-averaged velocity $-q$ (along the downward Ox-axis) imposed on our fluidized suspensions. The composition of the velocities leads, for the large beads, to

$$v_d = U_l - q. \tag{3}$$

This equation may be completed by a 'quasi-stationary state assumption', which expresses the condition obtained after the initial reconcentration (nearly constant height of the fluidized suspension). This height must then correspond to concentration conditions of null average flux of the particles:

$$\Phi_l(U_l - q) + \Phi_s(U_s - q) = 0. \tag{4}$$

We note that the above equation cannot be rigorously true, as it would mean that any profile of $\bar{\Phi}$, initially uniform, should remain uniform. This assertion cannot hold during the

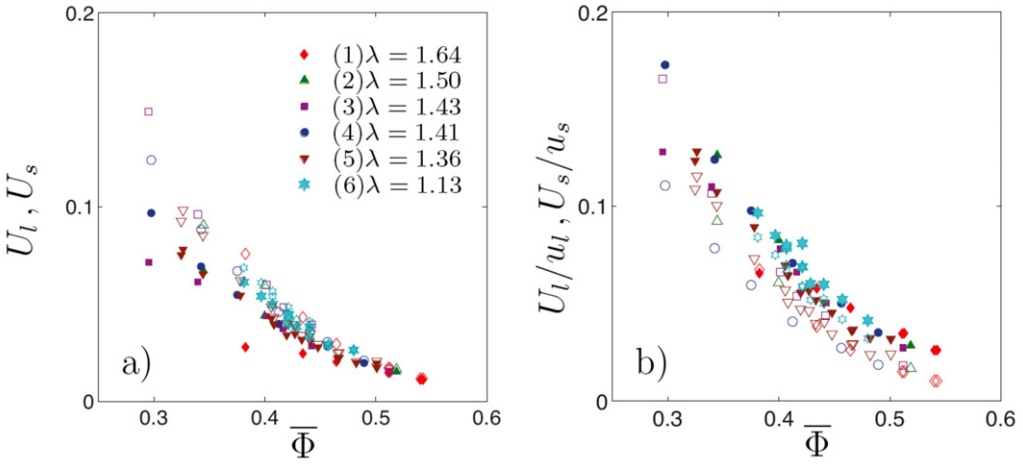

Figure 7. Sedimentation velocities, U_s and U_l, of the large and small beads inside the bidisperse suspensions, filled and open symbols, respectively, in mm s^{-1} (a) and normalized by the Stokes velocity u_l and u_s (b). Each symbol corresponds to one value of the size ratio λ, as in figure 6.

segregation phase, as the final concentrations, at a given q, differ in the two monodisperse suspensions. However, equation (4) is a good approximation and leads, with equation (2), to

$$q = (U_l + U_s)/2. \tag{5}$$

It is worth noting that, using equations (3) and (5), $v_d/q = 2(U_l - U_s)/(U_l + U_s)$, displayed in figure 6(b), is indeed twice the segregation velocity contrast. In a corresponding batch sedimentation experiment, the ratio of the final height of the segregated monodisperse suspension of small particles to the height of the initial suspension can be fairly estimated by $v_d/(2q)$. It follows from our measurements, $v_d/q < 0.08$ for $\bar{\Phi} \geqslant 0.5$, that at such high concentrations, for a size ratio $\lambda \leqslant 1.64$, the top segregated layer in a batch experiment is expected to be less than 4% (and even less for smaller λ values) of the settling height. This may explain the segregation inhibition, reported for concentrated batch experiments [26]. We note that equations (3) and (5) also enable us to estimate U_l and U_s from the measurements of the downward front velocity, v_d, and the surface flow rate q:

$$U_l = q + v_d \quad \text{and} \quad U_s = q - v_d. \tag{6}$$

The corresponding values of U_l and U_s are displayed in figure 7(a), together with their normalized counterparts, U_l/u_l and U_s/u_s, which are expected to depend on Φ_l, Φ_s and on the size ratio λ [9]. In our cases, as the bidisperse composition is fixed (equation (2)), the so-normalized sedimentation velocities, displayed in figure 7(b), should only depend on $\bar{\Phi}$ and λ. General trends can be noted in the different series displayed in figure 7. As expected, U_l and U_s decrease with $\bar{\Phi}$ (hindrance effect), and the sedimentation velocity difference, $(U_l - U_s)$, increases with increasing size ratio, λ (due to the Stokes velocity pre-factor). We also note that $(U_l - U_s)$ strongly decreases with $\bar{\Phi}$ and approaches zero for $\bar{\Phi} \geqslant 0.5$, whatever the λ value is. More interesting is the normalized representation of figure 7(b), which displays the hindering functions. We note that such a normalized representation reduces the large differences, which

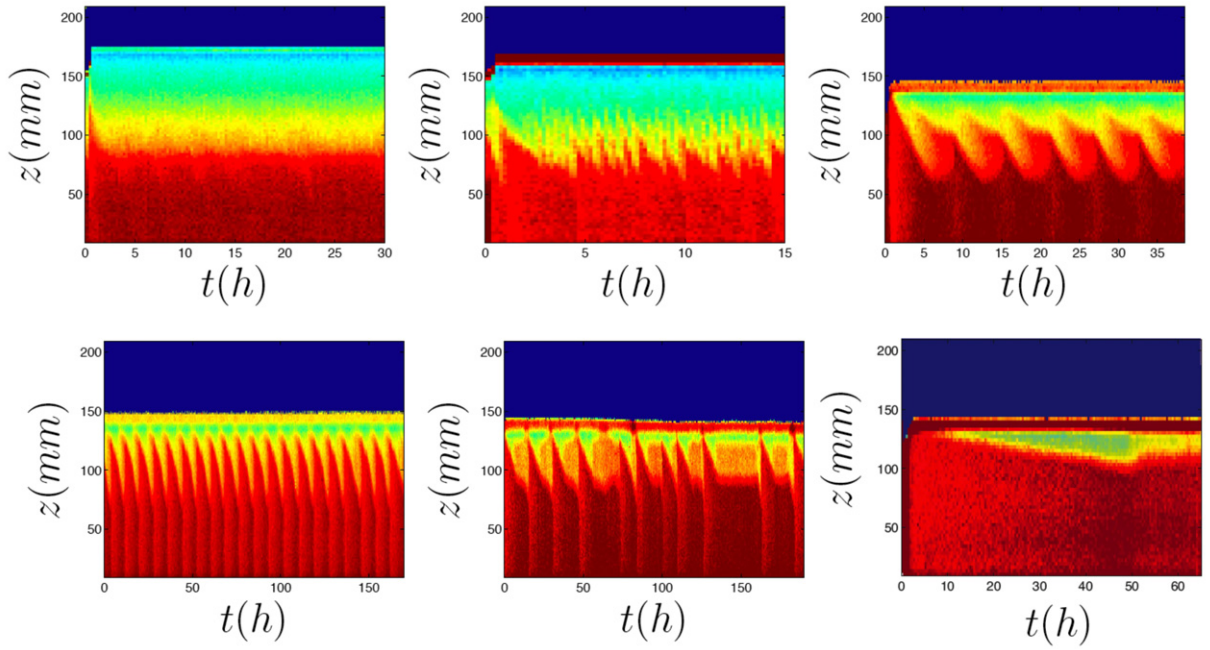

Figure 8. Spatiotemporal attenuation diagrams obtained with the bidisperse suspension 6, $\lambda = 1.13$, at $\bar{\Phi} = 0.26$, 0.34, 0.395, 0.415, 0.425 and 0.475, from left to right and top to bottom.

are observed in figure 7(a) at small $\bar{\Phi}$ and for the three sets of large λ (suspensions 1–3). This trend is in line with the collapse (onto the value 1) of the hindering functions expected at $\bar{\Phi} = 0$. However, rather constant differences between U_l/u_l and U_s/u_s are obtained, for each λ set, in the explored range $\bar{\Phi} \geqslant 0.3$. Also note that U_s/u_s is greater than U_l/u_l, systematically, which was of course expectable at large $\bar{\Phi}$, from the vanishing of the velocity differences $(U_l - U_s)$. However, the important point is that, for all our values of λ and up to concentrations even higher than 50%, the hierarchy $U_l > U_s$ always holds; $(U_l - U_s)$, and thus v_d, remain finite, so that long-term fluidization should always result in a segregated state and should thus provide an efficient (although slow) separation process.

4. Intermittency of segregation and mixing phases

4.1. Unsteady long-term fluidization

To address the issue of the separation efficiency, we carried out long-term fluidization of the suspension 6 ($\lambda = 1.13$), at high $\bar{\Phi}$. Typical spatiotemporal attenuation diagrams are displayed in figure 8. They exhibit totally unexpected behavior, as neither segregation nor inhibition is observed for intermediate values of $\bar{\Phi}$. Long-term fluidization results in the quasi-periodic intermittency of segregation and mixing phases, as displayed in the third and fourth diagrams of figure 8, measured at $\bar{\Phi} = 0.395$ and $\bar{\Phi} = 0.415$, respectively. In the latter case, the slow segregation sequence (several hours long) is longer than the mixing one, which looks nearly instantaneous on such time scales. In addition, we note that the mixing extends over the full height of the fluidized suspension. These features were rather common to the quasi-periodic

intermittency we observed. However, for lower $\bar{\Phi}$ values, as for $\bar{\Phi} = 0.395$, we note that slower mixing phases could be observed. The general trends observed when the value of $\bar{\Phi}$ was further decreased were the following: the segregation process became shorter and shorter (in accordance with the increase in the segregation velocity observed in figure 6); the intermittency became less and less periodic and the mixing phases involved a smaller and smaller extent of the suspension. In this way, for the smaller value $\bar{\Phi} = 0.26$ displayed in figure 8, the result of a long-term fluidization looks as a stationary diffuse segregated state, displaying a large and noisy frontier. We note that quasi-periodic intermittency was also observed for larger size ratios in suspensions 4 and 5 ($\lambda = 1.41$ and $\lambda = 1.36$), but in less extended ranges, [0.39, 0.42] and [0.38, 0.53], respectively. Such observations raise two major questions: What fixes the intermittency time and what is the origin of the mixing process?

4.2. Origin of the mixing

The suddenness and quickness of the mixing process make one think of an instability phenomenon. A good candidate can be the streaming instability, which has been observed during the batch sedimentation of bidisperse suspensions, in the presence of a density contrast between particles [27–29]. We note that our scanner measures the axial composition and is not designed to detect any transverse heterogeneity. Accordingly, a fast mixing induced by the onset of a streaming instability might result in the measured profiles. Although the existence of such a streaming instability could not be checked in our opaque fluidized suspensions, we did test the model proposed by Batchelor and Janse van Rensburg [29]. These authors suggested that the streaming instability could result from the hyperbolic–elliptic transition of the set of equations describing the axial evolution of the bidisperse system [29, 31, 32]. For given particle species, such a transition should occur at the composition frontier ($\Phi_l^\star$, $\Phi_s^\star$) delineating the hyperbolic and elliptic domains. Accordingly, the intermittency of segregation and mixing could be explained as follows: from an initially mixed state ($\Phi_l = \Phi_s = \bar{\Phi}/2$), the segregation process results in the development of a bottom bidisperse suspension of increasing Φ_l and decreasing Φ_s (as $\Phi_l + \Phi_s = \bar{\Phi}$ is almost constant). Then, destabilization and mixing occur when the composition reaches the frontier ($\Phi_l^\star$, $\Phi_s^\star$). We note that this criterion should correspond to a given height of the bottom bidisperse suspension, that is, to a given travel of the downward front and hence to a given segregation duration. As a result, the slow segregation phase should be interrupted by quick mixing phases at regular times, which indeed corresponds to our observations. We have tested this model by doubling the number of small particles in the column, at a fixed large particle load. As the number of large particles, all contained in the bottom bidisperse suspension, remained unchanged, the composition ($\Phi_l^\star$, $\Phi_s^\star$) was expected to be reached for the same height (i.e. the same volume) of the bottom bidisperse suspension. Unfortunately, our experiments showed that an increase in the number of small beads led to an increase of the segregation front position at the onset of mixing, which invalidates the hyperbolic–elliptic transition model. One may then invoke the depletion forces existing in bidisperse suspensions [42, 43] as an alternative destabilizing phenomenon. However, it remains an open question whether the resulting attraction between large particles is sufficient for overcoming the hydrodynamic dispersion induced by the settling [44]. We also note that the mixing phase could be triggered by the onset of gravitational instabilities resulting from the formation of an unstable density gradient in the fluidized suspension. This possibility has been explored with the help of time-of-flight measurements, which indeed provide the density

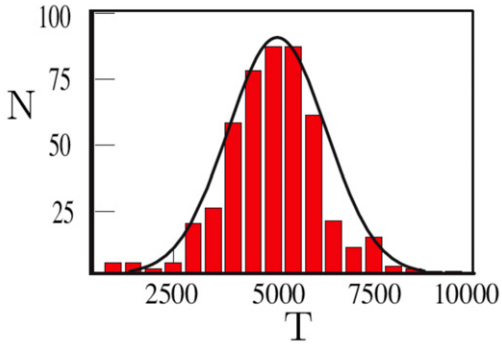

Figure 9. Distribution of 500 intermittency times, $T(s)$, measured in the suspension 5 ($\lambda = 1.36$), at $\bar{\Phi} = 0.37$.

profiles (through $\bar{\Phi}(z)$). The formation of such an unstable gradient has never been noted in our experiments. In contrast, during the segregation phases, $\bar{\Phi}(z)$ evolves slightly toward a more stable configuration, so the nature of the destabilizing process remains an open issue. We have, nevertheless, tried to characterize the intermittency time. Its statistics has been studied in the case of quasi-periodic behavior of suspension 5 at $\bar{\Phi} = 0.37$. The measured distribution, displayed in figure 9, is clearly Gaussian, and its large width indicates that the intermittency is indeed noisy and that the system cannot be described as a sharp resonator.

4.3. Intermittency time

However, the mean intermittency time is a good candidate to qualify the time scale of the system. We have measured the intermittency time in the fluidized suspension 6 at different volume fractions $\bar{\Phi}$ by averaging about ten quasi-periods. As the intermittency time is likely to be dominated by the segregation process, the measurements displayed in figure 10 are normalized by H_{susp}/u_1, which is the settling time of one large particle over the height of the suspension H_{susp} (which is the larger length of our system).

The relevance of such a normalization has been tested by using different fluid viscosities ($\eta = 30, 20, 17$ mPa s, obtained at different temperatures, 20, 25 and 30 °C). The good collapse of the normalized data supports the scaling with a low-Reynolds-number sedimentation time. However, we note that the normalized intermittency time becomes very long for $\bar{\Phi}$ exceeding 40%. Indeed, the data alignment in the log-linear representation of figure 10(b) suggests an exponential behavior of the intermittency time. Note that this behavior was also observed for suspension 5, up to a concentration as high as $\bar{\Phi} = 0.53$. Still, we note that such an increase is actually in line with the above-mentioned vanishing of the segregation velocity at large $\bar{\Phi}$, as we recall that the latter was found to decrease more strongly than the expected hindering functions (see figure 6). Moreover, as the intermittency time increases at large $\bar{\Phi}$, it also becomes more and more noisy (see ranges of measurements in figure 10). This is indeed a general trend observed in the oscillating suspensions: the intermittency becomes less and less regular as $\bar{\Phi}$ exceeds 40%. Its qualitative evolution is well illustrated by the diagram at $\bar{\Phi} = 0.425$, displayed in figure 8. The dispersion in the intermittency is mostly due to the appearance of 'unstable stationary phases', which do not correspond to the expected segregated state, as the frontier is too high for the bottom suspension to be a large beads monodisperse suspension. These states rather

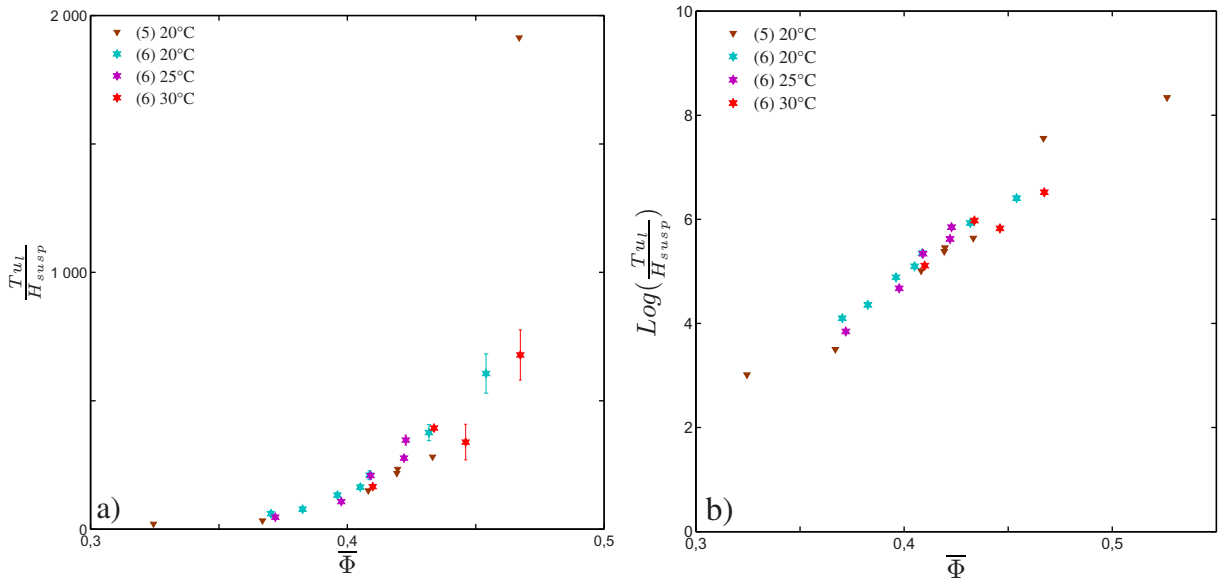

Figure 10. Evolution of the intermittency time, normalized by H_{susp}/u_1, with the volume fraction $\bar{\Phi}$, measured in the bidisperse suspensions 5 ($\lambda = 1.36$) and 6 ($\lambda = 1.13$). For suspension 6, data were collected at three different temperatures: 20, 25 and 30 °C (i.e. for three different fluid viscosities). The error bars indicate the actual range of measurements obtained during ten intermittencies.

correspond to partially segregated suspensions, with a bottom bidisperse suspension, enriched in large beads, and a top monodisperse suspension of small beads. These partially segregated states behave as metastable states or glassy states, and may hold for a rather long time (about 20 h for the last but one occurrence in the diagram at $\bar{\Phi} = 0.425$). This behavior is reminiscent of different phenomena, such as intermittency of cessations and reversals of circulation, reported in experiments on turbulent thermal convection [45], or granular avalanches [46], in which an exponential distribution of times was observed. However, the time scales of both the segregation phases and the 'metastable states' become too long at large $\bar{\Phi}$ to carry out any statistical study. It is even very difficult (and time-consuming) to discriminate between stationarity and intermittency, as illustrated by the case $\bar{\Phi} = 0.475$, displayed in figure 8, for which the result of long-term fluidization remained an open question after more than 60 h of experiment.

We note, however, that we did observe a rather convincing stationary segregated state at a very high concentration $\bar{\Phi} = 0.48$, in the suspension 5 ($\lambda = 1.36$), which is displayed in figure 11. In this experiment, the initial segregation process, of about 100 h long, resulted in a fully segregated state, which still lasted for 200 h. This could indicate that, unlike the partially segregated states, the fully segregated states could be stable. This is substantiated by the observation of intermittency, for the same suspension 5, at volume fractions either smaller or higher than $\bar{\Phi} = 0.48$, in experiments which differed in the initial conditions (i.e. no initial mixing) and in which no fully segregated state was ever achieved. However, such a statement has to be mitigated by time scale considerations: however convincing the stationarity of the diagram of figure 11 may be, the experiment is not longer than about twice the segregation time scale, and it cannot be taken for granted that some destabilization could not appear later.

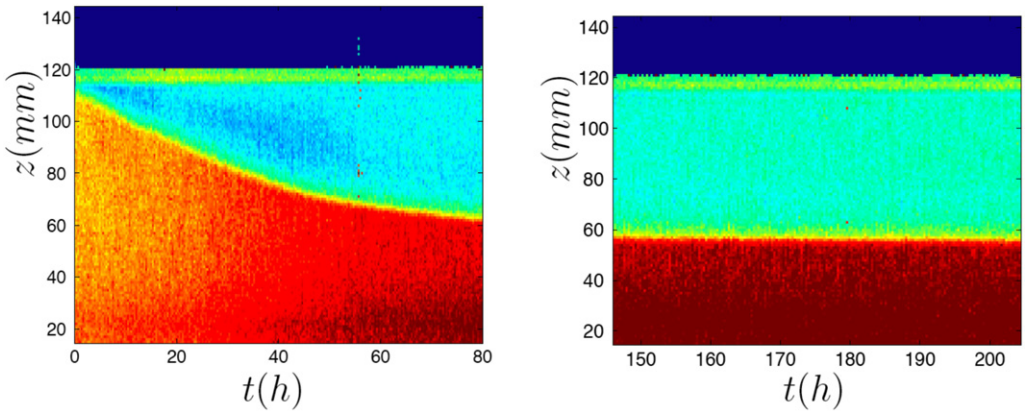

Figure 11. Spatiotemporal attenuation diagrams obtained with the bidisperse suspension 5 ($\lambda = 1.36$), at $\bar{\Phi} = 0.48$.

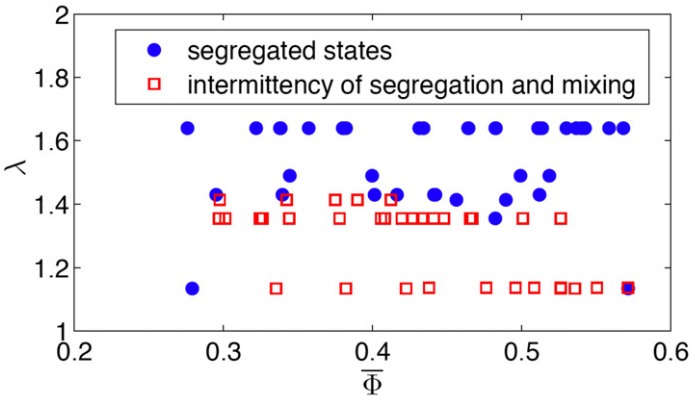

Figure 12. Diagram of the long-time behavior observed in bidisperse fluidized suspensions, as a function of the mean concentration $\bar{\Phi}$ and the size ratio λ.

5. Concluding remarks

The issue of segregation has been addressed in fluidized bidisperse suspensions of glass beads. An acoustic technique has been designed to acquire the axial composition along the fluidization column. From the analysis of the transient segregation fronts, we have collected precise measurements of the sedimentation velocities of the small and large beads, U_s and U_l, in homogeneous suspensions at the same volume fractions $\bar{\Phi}/2$ for both bead species, and for different size ratios $1.13 < \lambda < 1.64$, and solid concentrations $25\% < \bar{\Phi} < 50\%$. In agreement with recent batch sedimentation experiments [35], our measurements give evidence of a difference in the sedimentation velocities, U_s and U_l, for a size ratio as low as 1.15 and concentrations as high as 50%. These results make one expect that a long-term fluidization should then result in a stationary segregated state. This was indeed obtained for large particle size ratios λ, but at high concentration and for particles of close sizes, we surprisingly observed a pseudo-periodic intermittency of a segregation and a mixing phase, with a pseudo-period much longer than the batch sedimentation time.

The two different types of long-term fluidization behavior, collected in the six bidisperse suspensions, have been gathered in the plane ($\bar{\Phi}$, λ) displayed in figure 12. Although the

intermittency delineation at high $\bar{\Phi}$ remains questionable, as already discussed, the frontier $\lambda \simeq 1.4$ looks reliable. Indeed, whereas intermittency has been observed in the suspension 4 ($\lambda = 1.41$), the long-term fluidization of the suspension 3 ($\lambda = 1.43$) has always resulted in stationary full segregated states. However, this drastic discrimination in λ should certainly be mitigated in light of the size distributions displayed in figure 2. The distributions of the small and large particles of suspensions 4–5 exhibit a clear overlap, whereas those of suspensions 1–3 are actually bidisperse (discontinuous). It is likely that this difference might be the relevant criterion to explain the intermittency appearance. Indeed, the presence of a continuous distribution of Stokes velocities will definitely help mixing, whatever the underlying mechanism.

Acknowledgments

This work was partly supported by the Agence Nationale de la Recherche 'Co-Liner', CNES (No. 793/CNES/00/8368), by ESA (No. AO-99-083) and by the Réseaux de Thématiques de Recherches Avancées 'Triangle de la physique'. AD was supported by a grant from the French Ministry of Research (MESR). All these sources of support are gratefully acknowledged.

References

[1] Koch D L and Shaqfeh E S G 1989 The instability of a dispersion of sedimenting spheroids *J. Fluid Mech.* **209** 521–42
[2] Ham J M and Homsy G M 1988 Hindered settling and hydrodynamic dispersion in quiescent sedimenting suspensions *Int. J. Multiph. Flow* **14** 533–46
[3] Nicolai H, Herzhaft B, Hinch E J, Oger L and Guazzelli E 1995 Particle velocity fluctuations and hydrodynamic self-diffusion of sedimenting non-Brownian spheres *Phys. Fluids* **7** 12
[4] Kynch G J 1952 A theory of sedimentation *Trans. Faraday Soc.* **48** 166–76
[5] Bacri J-C, Frenois C, Hoyos M, Perzynski R, Rakotomalala N and Salin D 1986 Acoustic study of suspension sedimentation *Europhys. Lett.* **2** 123
[6] Auzerais F M, Jackson R and Russel W B 1988 The resolution of shocks and the effects of compressible sediments in transient settling *J. Fluid Mech.* **195** 437–62
[7] Martin J, Rakotomalala N and Salin D 1995 Accurate determination of the sedimentation flux of concentrated suspensions *Phys. Fluids* **7** 2510–2
[8] Dorrell R and Hogg A J 2010 Sedimentation of bidisperse suspensions *Int. J. Multiph. Flow*
[9] Batchelor G K 1982 Sedimentation in a dilute polydisperse system of interacting spheres. Part 1. General theory *J. Fluid Mech. Dig. Arch.* **119** 379–408
[10] Batchelor G K and Wen C S 1982 Sedimentation in a dilute polydisperse system of interacting spheres. Part 2. numerical results *J. Fluid Mech. Dig. Arch.* **124** 495–528
[11] Lockett M J and Al-Habbooby H M 1974 Relative particle velocities in two-species settling *Powder Technol.* **10** 67–71
[12] Masliyah J H 1979 Hindered settling in a multi-species particle system *Chem. Eng. Sci.* **34** 1166–8
[13] Mirza S and Richardson J F 1979 Sedimentation of suspensions of particles of two or more sizes *Chem. Eng. Sci.* **34** 447–54
[14] Funamizu N and Takakuwa T 1996 A minimal potential energy model for predicting stratification pattern in binary and ternary solid–liquid fluidized beds *Chem. Eng. Sci.* **51** 341–51
[15] Patwardhan V S and Tien C 1985 Sedimentation and liquid fluidization of solid particles of different sizes and densities *Chem. Eng. Sci.* **40** 1051–60
[16] Davis R H and Gecol H 1994 Hindered settling function with no empirical parameters for polydisperse suspensions *AIChE J.* **40** 1547–905

[17] Cheung M K, Powell R L and McCarthy M J 1996 Sedimentation of noncolloidal bidisperse suspensions *AIChE J.* **42** 271–6
[18] Smith T N 1997 Differential settling of a binary mixture *Powder Technol.* **92** 171–8
[19] Koo S and Sangani A S 2002 Effective-medium theories for predicting hydrodynamic transport properties of bidisperse suspensions *Phys. Fluids* **14** 3522
[20] Krishnamoorthy P, Reghupathi I and Murugesan T 2007 An experimental study and correlation for differential settling of bidisperse suspensions *Chem. Biochem. Eng. Q.* **21** 241–50
[21] Lockett M J and Al-Habbooby H M 1973 Differential settling by size of two particle species in a liquid *Chem. Eng. Res. Des.* **51** 281–92
[22] Selim M S, Kothari A C and Turian R M 1983 Sedimentation of multisized particles in concentrated suspensions *AIChE J.* **29** 1029–38
[23] Davis R H and Birdsell K H 1988 Hindered settling of semidilute monodisperse and polydisperse suspensions *AIChE J.* **34** 123–9
[24] Bruneau D, Anthore R, Feuillebois F, Auvray X and Petipas C 1990 Measurement of the average velocity of sedimentation in a dilute polydisperse suspension of spheres *J. Fluid Mech. Dig. Arch.* **221** 577–96
[25] Al-Naafa M A and Selim M S 1992 Sedimentation of monodisperse and bidisperse hard-sphere colloidal suspensions *AIChE J.* **38** 1618–30
[26] Hoyos M, Bacri J-C, Martin J and Salin D 1994 A study of the sedimentation of noncolloidal bidisperse, concentrated suspensions by an acoustic technique *Phys. Fluids* **6** 3809
[27] Whitmore R L 1955 The sedimentation of suspensions of spheres *Br. J. Appl. Phys.* **6** 239–45
[28] Weiland R H, Fessas Y P and Ramarao B V 1984 On instabilities arising during sedimentation of two-component mixtures of solids *J. Fluid Mech.* **142** 383–9
[29] Batchelor G K and Janse Van Rensburg R W 1986 Structure formation in bidisperse sedimentation *J. Fluid Mech.* **166** 379–407
[30] Abbas M, Climent E, Simonin O and Maxey M R 2006 Dynamics of bidisperse suspensions under Stokes flows: linear shear flow and sedimentation *Phys. Fluids* **18** 121504
[31] Biesheuvel P M, Verweij H and Breedveld V 2001 Evaluation of instability criterion for bidisperse sedimentation *AIChE J.* **47** 45–52
[32] Shariati M, Talon L, Martin J, Rakotomalala N, Salin D and Yortsos Y C 2004 Fluid displacement between two parallel plates: a non-empirical model displaying change of type from hyperbolic to elliptic equations *J. Fluid Mech.* **519** 105–32
[33] Moritomi H, Iwase T and Chiba T 1982 A comprehensive interpretation of solid layer inversion in liquid fluidised beds *Chem. Eng. Sci.* **37** 1751–7
[34] Di Felice R 1995 Hydrodynamics of liquid fluidisation *Chem. Eng. Sci.* **50** 1213–45
[35] Snabre P, Pouligny B, Metayer C and Nadal F 2009 Size segregation and particle velocity fluctuations in settling concentrated suspensions *Rheol. Acta* **48** 855–70
[36] Martin J, Rakotomalala N and Salin D 1995 Hydrodynamic dispersion of noncolloidal suspensions: measurement from Einstein's argument *Phys. Rev. Lett.* **74** 1347–50
[37] Segré P N 2002 Origin of stability in sedimentation *Phys. Rev. Lett.* **89** 254503
[38] Segré P N and McClymer J P 2004 Fluctuations, stratification and stability in a liquid fluidized bed at low Reynolds number *J. Phys.: Condens. Matter* **16** 4219–30
[39] Tee S Y, Mucha P J, Brenner M P and Weitz D A 2008 Velocity fluctuations in a low-Reynolds-number fluidized bed *J. Fluid Mech.* **596** 467–75
[40] Bacri J-C, Hoyos M, Rakotomalala N, Salin D, Bourlion M, Daccord G, Lenormand R and Soucemarianadin S 1991 Ultrasonic diagnostic in porous media and suspensions *J. Physique* III **1** 1455–66
[41] Richardson J F and Zaki W N 1954 The sedimentation of a suspension of uniform spheres under conditions of viscous flow *Chem. Eng. Sci.* **3** 65–73
[42] Asakura S and Oosawa F 1954 On interaction between two bodies immersed in a solution of macromolecules *J. Chem. Phys.* **22** 1255–6

[43] Ramaswamy S 2001 Issues in the statistical mechanics of steady sedimentation *Adv. Phys.* **50** 297–341
[44] Peysson Y and Guazzelli E 1999 Velocity fluctuations in a bidisperse sedimenting suspension *Phys. Fluids* **11** 1953
[45] Xi H D and Xia K Q 2007 Cessations and reversals of the large-scale circulation in turbulent thermal convection *Phys. Rev.* E **75** 66307
[46] Fischer R, Gondret P and Rabaud M 2009 Transition by intermittency in granular matter: from discontinuous avalanches to continuous flow *Phys. Rev. Lett.* **103** 128002